



Geochemical Behaviour of Rare Earth Elements Throughout an Acid Mine Drainage Passive Treatment System in the Lousal Mine Area, Portugal

Cynthia Obregón-Castro¹ · Maria Isabel Prudêncio¹ · Catarina Diamantino³ · Edgar Carvalho³ · Dulce Russo^{1,2} · Rosa Marques^{1,2}

Received: 2 May 2023 / Accepted: 6 September 2023 / Published online: 4 October 2023

© The Author(s) 2023

Abstract

A passive remediation system was installed between 2010 and 2015 at the Lousal legacy mine site in southwestern Portugal to minimize the impact of AMD. This is the first study of the geochemical behaviour of rare earth elements (REE) in the area after implementation of the passive treatment system. The total and dissolved concentrations of REE is similar throughout the basins/wetlands and acidic ponds in both sampling campaigns, which is mainly attributed to the conservative behaviour of these elements in acidic water. In areas where mixing of acidic and circumneutral water occurs, the REE were partially removed from solution by adsorption onto newly formed Al and Fe precipitates. Sorption onto the precipitates varies between the rare earths, with a preferential fixation of heavy REE (HREE) compared to the light REE (LREE). The normalized distribution patterns exhibit the characteristic convex-up enrichment in middle rare earth elements for AMD and display an enrichment of LREE relative to HREE in areas where mixing of waters occurs, and the pH is close to circumneutral.

Keywords REE · Geochemistry · AMD · Hydrochemistry · Particulate matter

Introduction

The production of acid mine drainage (AMD) from abandoned mines is a major environmental problem (Ferreira da Silva et al. 2009; Valente et al. 2012). The exposure of sulphide minerals (mainly pyrite) to atmospheric conditions generates acidity and sulphate, and can liberate high concentrations of Fe, trace metals, and rare earth elements (REE), which can contaminate the soils, groundwaters, and surface waters in the surrounding area (Cánovas et al. 2006). The REE are a group of 17 chemical elements with similar chemical properties and geochemical behaviour (Gromet

et al. 1984; Henderson 1984), comprising the lanthanides plus scandium and yttrium (IUPAC 2005). The geochemistry of REE in the interpretation of water–rock interactions has been extensively studied, gaining attention as potential tracers in acidic mine waters environments and controlling the transportation of metals (e.g. Alpers et al. 1994; Åström et al. 2009; Fernández-Caliani et al. 2009; Ferreira da Silva et al. 2009; Johannesson and Lyons 1995; Johannesson and Zhou 1999; Leybourne and Johannesson 2008; Li and Wu 2017; Prudêncio et al. 2015; Verplanck et al. 1999; Worral and Pearson 2001).

Passive treatment systems (PTS) have been implemented for AMD remediation to remove metals and acidity by taking advantage of naturally occurring chemical and biological processes (Skousen et al. 2017). The pH of the water is one of the most important parameters, as it affects the mobility as well as the speciation of a range of chemical elements. Rare earth elements generally have a higher mobility in acidic rather than in neutral or alkaline waters (Ferreira da Silva et al. 2009; Noack et al. 2014; Olías et al. 2018). Al is mainly transported in the dissolved form in acidic conditions and as particulate matter at circumneutral pH values (Cánovas et al. 2018). Similar

✉ Cynthia Obregón-Castro
cynthia.castro@ctn.tecnico.ulisboa.pt

¹ Centro de Ciências e Tecnologias Nucleares (C2TN), Instituto Superior Técnico, EN 10 (Km 139,7), 2695-066 Bobadela, Portugal

² Departamento de Engenharia e Ciências Nucleares (DECN), Instituto Superior Técnico, EN 10 (Km 139,7), 2695-066 Bobadela, Portugal

³ EDM-Empresa de Desenvolvimento Mineiro SA (EDM), Rua Sampaio e Pina, nº1, 7º, 1070-248 Lisbon, Portugal

behaviour has been reported for Σ REE concentrations in mining-associated surface waters in which the REE transport occurs mainly in dissolved forms at $\text{pH} < 3$ and in the particulate matter at $\text{pH} > 7$ (Olías et al. 2018). Fe is also found mostly in the particulate form at a pH above 6, but there is some variability in the amount of Fe in the suspended matter at acidic pH in AMD. The transportation of Fe in the particulate form depends on factors such as water velocity, which affect the suspension or sedimentation of the Fe oxyhydroxide and oxyhydroxisulphate particles in the water (Cánovas et al. 2018).

The Lousal pyrite mine, which operated in the twentieth century, is part of a polymetallic massive sulphide deposit located in southwestern Portugal. Several studies have been conducted in the area focusing on the geochemical characterization of the AMD discharge, soils, sediments, and surface waters, their interaction, and the extent of pollution (e.g. Ferreira da Silva et al. 2005, 2006; Luís et al. 2011). Ferreira da Silva et al. (2006) found that the mine tailings were composed mainly of quartz, feldspar, chlorite, muscovite, illite, and kaolinite, as well as hematite, ilmenite, pyrite, chalcopyrite, galena, and sphalerite.

In 2001, the Portuguese Government granted a concession contract to Empresa de Desenvolvimento Mineiro S.A. (EDM), a state-owned enterprise, for the characterization, assessment, and rehabilitation of environmentally affected abandoned mining areas in Portugal (Oliveira et al. 2002), including the Lousal legacy mine site. After the characterization and development of the projects, EDM started environmental remediation operations in the area in 2010 with the installation of an AMD passive treatment system downstream of the cementation cells, sealing of the shafts and tunnels, partial removal of mining waste and other residues, and the sealing of the open pit area, among other works. In 2014, another phase of the remediation operations included improvements in the passive treatment system, modelling and sealing of the old train loading platform and ore and waste rock pile, and installation of an underground seepage collection and drainage system. The PTS has been operating since 2014/2015. After almost 10 years, EDM plans to implement a complementary phase of remediation to improve the performance of the PTS and to install a continuous monitoring system.

Earlier work on REE undertaken by Ferreira da Silva et al. (2009) reported acidic waters flowing from the tailings with high dissolved sulphate concentrations (up to $20,070 \text{ mg L}^{-1} \text{ SO}_4^{2-}$) with enrichment in Al, Fe, and other trace elements. The Σ REE concentrations ranged between 345 to $1107 \text{ }\mu\text{g L}^{-1}$, the highest reported in Spring. After implementation of the PTS, regular monitoring has been

performed by EDM, although no publications related to the PTS and REE were found in the literature. This work is the first to present results of the distribution and behaviour of REE in the AMD and river water after the construction of the Lousal PTS.

The principal objectives of this study were: (i) to evaluate the geochemical behaviour of the water in the area, focusing on the REE distribution in the AMD and throughout the PTS, (ii) to establish the REE patterns and identify factors controlling the distribution of the REE in the AMD, PTS, and river water before and after AMD discharges, (iii) to quantify the dissolved and particulate metal fluxes in the different stages of the PTS and AMD, and (iv) to evaluate the seasonal behaviour of REE within the PTS.

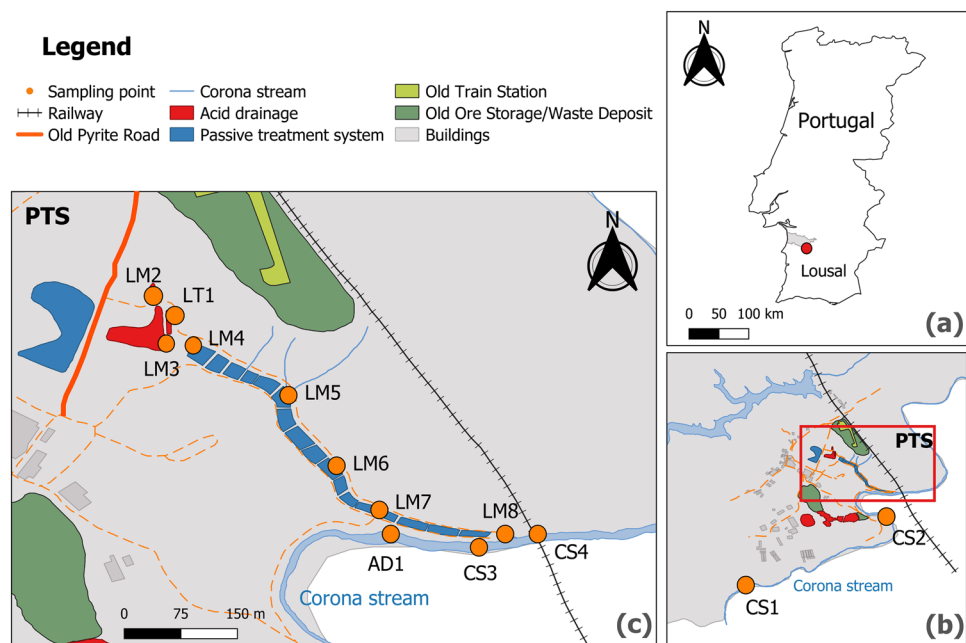
Study Area

The Lousal polymetallic sulphide mine is located in the northwestern sector of the Iberian Pyrite Belt (IPB), in the Grândola municipality, in southern Portugal (Fig. 1a). The geological units exposed in the area are: the phyllite-quartzite group (PQG)—Corona Formation consisting of phyllites, siltstones and quartzites; a volcanic sedimentary complex expressed by the shales, acid meta-vulcanites, diabases, jaspers, and cherts that host the Lousal massive sulphides; and a sedimentary sequence represented mainly by the Mertola Formation, which consists of turbidites, greywackes, siltstones, shales, and conglomerates (Luís et al. 2011).

The climate in the Grândola municipality is dry sub-humid with moderate water deficit in summer (Life Riber-mine 2021). The average temperature is $16.2 \text{ }^{\circ}\text{C}$, with the lowest temperature being registered between December and February (average $5 \text{ }^{\circ}\text{C}$), and the highest values between June and September (average $29 \text{ }^{\circ}\text{C}$). The highest precipitation occurs between October and December (average 80 mm/month) with 47% of the annual precipitation. The region is in a hydrological deficit with little precipitation, especially during the warmest months of the year, June and September (average 3 mm/month) (Camarâ Municipal de Grândola 2012).

Surface mining activities began in 1900 for pyrite and copper extraction from the main gossans and their supergene enrichment zones (Ferreira da Silva et al. 2005; Strauss 1970). Later, in the 1930s, underground mining took place in deeper orebodies to increase the production of pyrite concentrates (Ferreira da Silva et al. 2005; Matos and Oliveira 2003; Strauss 1970). The mineralization is dominated by pyrite; however, variable amounts of chalcopyrite, galena, sphalerite, pyrrhotite, other iron and copper sulphides, and native gold are present (Strauss 1970). The mine ceased

Fig. 1 **a** Location of the Lousal mine area (Grândola, Portugal); **b** sampling points in the Corona Stream, upstream the influence of the mine area (CS1, CS2); and **c** detail of the passive treatment system and sampling points (LT1, LM2–8) in the Lousal mine area, and in the Corona Stream (CS3, CS4, and AD1 -collected in an old outflow of AMD)



activities in 1988 with one main open-pit, several tunnels for underground mining, and large volumes of waste, including overburden and tailings impoundments.

The passive treatment system at the Lousal mine is located next to the confined waste rock deposit and comprises a freshwater pond, a seepage collection tank, a lined acidic pond, and 17 treatment basins (Fig. 1b, c). The freshwater comes from the Tapada Dam Reservoir, located in the northwestern part of the complex. This source is used to feed the treatment system, ensuring that water is always flowing, especially during the dry season. A watertight pond collects the AMD seepage from the historic pyritic road, which was capped with clay (Fig. 1c). Connected to the main acidic pond, there is a tributary seasonal pond that used to collect drainage from the ore loading platforms and waste rock deposit; it does not have a liner and depends on the amount of rain and evaporation. A sub-superficial drainage system collects water from the confined deposit, which used to be the old ore storage and loading platform and waste rock pile. The acidic seepage from the capped deposit is conducted to the seepage collection tank and discharges directly to the first pond of the wetland system.

The passive treatment basins consist of five aeration and sedimentation ponds, and 12 aerobic wetlands with planted macrophytes used for treatment rectification. There is a limestone barrier between each basin to create a permeable dike and a layer of rocks with limestone in the bottom of each basin. The whole system was designed as a gravity-driven cascade and confined with a HDPE geomembrane. In the

basins with the planted macrophytes, there is a layer of limestone and/or clay beneath the topsoil (Fig. 1c).

Materials and Methods

Twenty-five water samples were collected in the Lousal mine area from AMD inputs, ponds throughout the PTS, and upstream and downstream of the PTS outflow to the Corona Stream (Fig. 1 and Table 1). Aside from sample LM7, all of the samples were collected from the surface of the waterbodies. Sample LM7 was collected from the outflow of a HDPE tube that collects the water from beneath the basin. To evaluate seasonal behaviour, the sampling was performed in two different campaigns, during Autumn (November 2020) and Spring (May 2021), representing the beginning of the wet (WS) and dry seasons (DS), respectively. Samples were collected at the same locations in both campaigns, with the exception of the WS/LM8 and DS/LM8 samples. Due to the lack of water flowing to the Corona Stream, the DS/LM8 sample was collected in the last wetland instead of the output of the PTS. During the dry season, one sample was also collected from an old AMD outflow (from before the construction of the PTS) to the Corona Stream (AD1 in Fig. 1c). Temperature (T), pH, oxidation-reduction potential (ORP), and electrical conductivity (EC), among other physicochemical parameters, were measured on site at each sampling location using the Aquaprobe AP-2000 multiparameter probe, which was

Table 1 Seasonal distribution of physicochemical parameters and sulphate concentration in water samples from the acidic ponds, passive treatment system and Corona Stream of Lousal mine area, Portugal

Sample	Ref	T °C	pH	EC μS cm ⁻¹	SO ₄ ²⁻ mg L ⁻¹	Sample	Ref	T °C	pH	EC μS cm ⁻¹	SO ₄ ²⁻ mg L ⁻¹
WS/LT1	1	17.6	2.3	3908	2800	DS/LT1	1	22.2	2.2	4044	2900
WS/LM2	2	18.2	2.9	1617	610	DS/LM2	2	24.7	2.4	3206	1700
WS/LM3	3	18.5	2.9	1622	670	DS/LM3	3	23.4	2.3	3132	1800
WS/LM4	4	20.9	2.9	2034	900	DS/LM4	4	23.4	2.4	3328	2100
WS/LM5	5	24.2	2.9	2326	1100	DS/LM5	5	28.7	2.7	3205	1900
WS/LM6	6	19.5	3.0	2226	1000	DS/LM6	6	28.2	2.7	3537	2200
WS/LM7	7	18.6	3.1	2256	1200	DS/LM7	7	20.7	5.2	3399	2200
WS/LM8	8	19.3	3.2	2393	1200	DS/LM8	8	29.8	2.9	4605	3000
WS/CS1	9	17.6	6.6	924	45	DS/CS1	9	24.1	6.6	319	36
WS/CS2	10	17.2	6.4	958	56	DS/CS2	10	23.2	5.9	710	46
WS/CS3	11	17.8	5.5	1649	560	DS/CS3	11	24.1	6.1	1190	267
WS/CS4	12	17.5	5.2	1709	590	DS/CS4	12	25.8	5.9	1209	239
						DS/AD1	13	24.7	2.9	3484	2300

WS wet season, DS dry season, LT1 Seepage Collection Tank, LM2-3 acidic ponds, LM4-8 Wetlands from the passive treatment system, CS1-4 Corona Stream, AD1 acidic seepage, Ref. Sample reference in the figures and graphs

calibrated using the equipment manufacturer's standard solution (Aquaprobe RapidCal solution).

The water samples for chemical analysis were collected with syringes and filtered in the field with 0.45 μm Milipore PES filters. Three set of samples were collected at each site: (i) unacidified for anion analysis, (ii) acidified to pH < 2 with HNO₃ suprapur (2%) for total element concentrations, and (iii) filtered and acidified to pH < 2 with HNO₃ suprapur (2%) for dissolved element concentrations. All of the samples were stored at 4 °C prior to laboratory analysis. The particulate fraction was estimated from the difference in concentrations between the total and filtered samples.

Major anions (Cl⁻, NO₃⁻, SO₄²⁻) were analysed at Laboratório de Análises do Instituto Superior Técnico (LAIST) in Portugal. The analysis of major, trace, and REE total and dissolved elements were performed by inductively coupled plasma-optical emission spectroscopy (ICP-OES), and inductively coupled plasma-mass spectrometry (ICP-MS) at Activation Laboratories Ltd. (Actlabs) in Canada, accredited under ISO/IEC 17025:2017. The detection limit ranged between 700 to 2 μg L⁻¹ for the major elements, such as Al, Ca, Fe, Mg, Na, K, and Si; and 0.001 μg L⁻¹ for the REE. The accuracy of the analyses was compared with the certified reference material IV-STOCK-1643 (Inorganic Ventures), along with several duplicates and blanks.

For this work, La through Pr are considered light rare earth elements (LREE), Nd through Dy middle rare earth elements (MREE), and Ho to Lu heavy rare earth elements (HREE) (Sholkovitz 1995). To evaluate the REE fractionation in the AMD, PTS, and river water, REE concentrations were normalized using the Post-Archean Australian Shale (PAAS) values (Nance and Taylor 1976). The Ce and Eu anomalies were calculated using the equations Ce/Ce* = [(Ce_N)/(√(La_N × Pr_N))] and Eu/Eu* = [(Eu_N)/(√(Sm_N × Gd_N))] (Worral and Pearson 2001). Relative REE enrichment was evaluated using the following ratios: LREE/HREE and LREE/MREE enrichments by (La/Yb)_N and (La/Gd)_N.

Results and Discussion

Physicochemical Parameters

The physicochemical parameters and sulphate concentrations in the water samples from the acidic ponds, PTS, and Corona Stream are given in Table 1. During the wet season, the average temperature in the AMD, PTS, and Corona Stream was 18.1, 20.5, and 17.5 °C, respectively. The measured pH in the acidic ponds and PTS water ranged from 2.3 to 3.2. Upstream of the confluence with

the PTS, the average pH of the Corona Stream was 6.5. Thereafter, it decreased to 5.5 after the input of an acidic seepage identified in the second campaign, and to 5.2 after the outflow of the PTS. The highest EC and SO_4^{2-} concentration values measured were from the seepage collection tank (WS/LT1). Throughout the PTS, excluding sample WS/LT1, both the EC and the SO_4^{2-} concentration increased before the water reached the Corona Stream. After the confluence, the EC and the SO_4^{2-} concentration declined (Table 1).

The water temperature during the dry season increased in the entire area, and especially in the PTS, with an average of 26.2 °C. The highest temperature reported was in the last wetland (DS/LM8). The pH was similar in the AMD and passive treatment system (2.2 to 2.9), with the exception of point DS/LM7, where a pH of 5.2 was measured. The pH of the Corona Stream was higher upstream of the influent AMD, similar to the wet season (6.6), and then slightly decreased downstream. Overall, the EC and SO_4^{2-} concentration were higher than during the wet season and highest at sampling point DS/LM8 (Table 1). The mean EC in the acidic ponds and wetlands was 3487 $\mu\text{S cm}^{-1}$ with an average SO_4^{2-} concentration of 2233 mg L⁻¹. The lower concentrations in the WS were due to dilution, as water flux along the system was greater than during the DS, when no water flowed from the PTS to the stream. The increase in the EC and SO_4^{2-} concentration in the river coincided with the input of the acidic seepage, but with no significant pH change (Table 1).

We used a modified Ficklin diagram (Plumlee et al. 1999), in which dissolved base metals concentrations are

plotted against pH values, to assess element concentrations. The seepage collection tank, acidic ponds, and PTS waters plot in the field of “High Acid, High Metal” and “Acid, High Metal” (Fig. 2). Total and dissolved concentrations of Al and Fe in the water samples from both seasons are shown in supplemental Table S-1. The highest concentrations in the wet season occurred in the seepage collection tank. The acidic ponds (WS/LM2 and WS/LM3) had similar concentrations in all elements in both total and dissolved phases. The waters from the acidic ponds (LM2, LM3) and the seepage collection tank (LT1) are mixed in the first aeration pond of the PTS (LM4). Most (94%) of the Al and Fe were dissolved, though sample DS/LM7 had much lower concentrations of Al and Fe, especially in the dissolved phase. The transport of Al (99%) was almost entirely as particulate matter, due to the increased pH at this point.

Water from the Corona Stream is classified as “Near Neutral, Low Metal”, while the water affected by the acidic seepage and the PTS was classified as “Near Neutral, High Metal” in the modified Ficklin diagram (Fig. 2). The transport of Al and Fe took place mainly in the particulate fraction throughout the river.

Rare Earth Elements

The total and dissolved concentrations of each REE in the water from the acidic mine ponds, aeration ponds, PTS, and Corona Stream are shown in supplemental Table S-2 and Table 2, respectively.

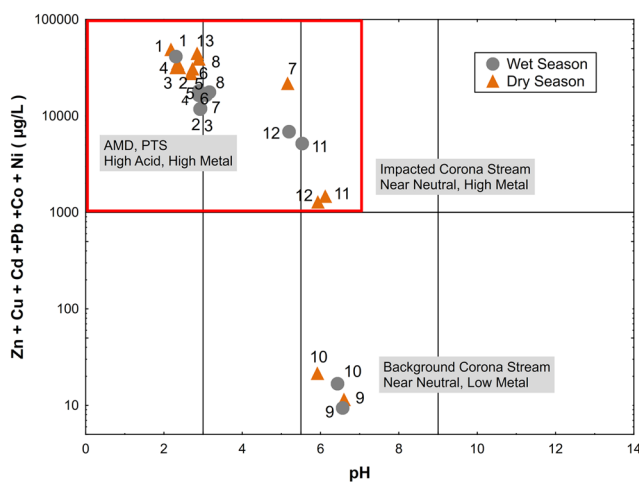
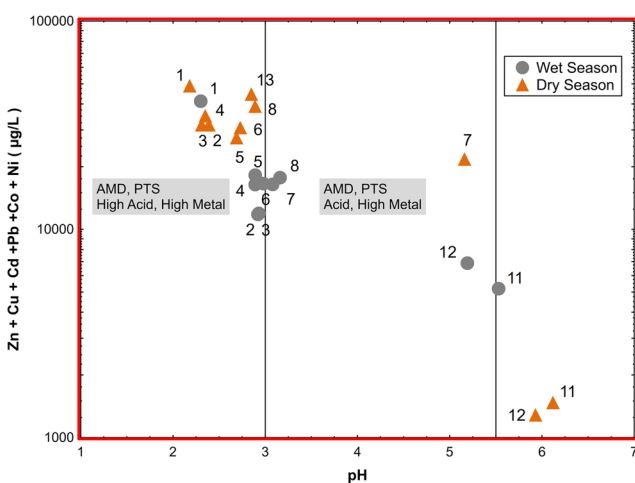


Fig. 2 Modified Ficklin diagram (Plumlee et al. 1999) for water samples of Lousal mine, Portugal. Samples labels 1–8 correspond to samples collected from the acidic ponds (AMD) and passive treatment system (PTS); sample labels 9, 10 correspond to samples collected



in the Corona Stream as background, sample labels 11, 12 represent water samples from the Corona Stream impacted by an acidic seepage and the PTS; sample label 13 corresponds to a water sample collected in the acidic seepage

Table 2 Seasonal distribution of REE concentration in the dissolved fraction in water samples from the acidic ponds, passive treatment system and Corona Stream of Lousal mine, Portugal

Sample	La µg L ⁻¹	Ce µg L ⁻¹	Pr µg L ⁻¹	Nd µg L ⁻¹	Sm µg L ⁻¹	Eu µg L ⁻¹	Gd µg L ⁻¹	Tb µg L ⁻¹	Dy µg L ⁻¹	Ho µg L ⁻¹	Er µg L ⁻¹	Tm µg L ⁻¹	Yb µg L ⁻¹	Lu µg L ⁻¹	ΣLREE µg L ⁻¹	ΣHREE µg L ⁻¹	ΣREE µg L ⁻¹	
WS/LT1	95.9	191	32.5	143	35.2	8.32	33.2	4.72	21.8	3.87	9.86	1.22	7.29	1.00	498	91	589	
WS/LM2	27.5	73.2	9.61	42.5	10.8	2.88	12.0	1.80	8.64	1.57	4.01	0.496	2.88	0.402	164	35	198	
WS/LM3	27.7	73.8	9.75	43.1	10.9	2.91	12.3	1.82	8.80	1.59	4.05	0.50	2.91	0.407	165	35	200	
WS/LM4	30.9	81.5	10.8	49.9	14.6	3.99	18.3	2.79	13.2	2.37	6.05	0.742	4.37	0.609	188	52	240	
WS/LM5	28.5	78.4	10.7	49.4	13.9	3.84	17.1	2.60	12.5	2.27	5.80	0.716	4.17	0.572	181	50	230	
WS/LM6	28.7	77.3	10.2	46.1	12.6	3.44	15.4	2.35	11.3	2.05	5.23	0.638	3.70	0.514	175	45	220	
WS/LM7	27.8	75.1	9.86	45.1	12.1	3.27	14.6	2.20	10.7	1.93	4.94	0.599	3.45	0.472	170	42	212	
WS/LM8	33.1	87.7	11.4	51.2	13.5	3.59	16.0	2.43	11.8	2.16	5.48	0.668	3.83	0.525	197	47	243	
WS/CS1	0.012	0.008	0.002	0.009	0.002	—	—	—	0.002	—	0.002	—	0.001	—	0.030	0.010	0.040	
WS/CS2	0.021	0.023	0.003	0.020	0.004	0.002	—	—	0.004	—	0.003	—	0.004	—	0.070	0.010	0.080	
WS/CS3	4.26	6.36	0.577	2.23	0.378	0.084	0.558	0.067	0.301	0.059	0.135	0.013	0.061	0.01	14	1.3	15	
WS/CS4	9.14	18.8	2.09	8.82	1.87	0.457	2.42	0.325	1.50	0.284	0.679	0.071	0.345	0.05	41	6.1	47	
DS/LT1	85.1	222	30.2	129	32.9	8.13	35.6	4.94	22.5	3.92	9.98	1.34	7.36	1.09	499	95	594	
DS/LM2	63.8	164	21.0	89.4	23.9	6.40	28.5	4.27	19.5	3.60	9.01	1.16	6.61	0.99	362	80	442	
DS/LM3	63.2	164	21.1	88.8	24.2	6.53	29.7	4.25	19.4	3.57	9.26	1.17	6.80	0.96	361	82	443	
DS/LM4	74.3	202	26.4	114	33.7	9.32	43.7	6.44	29.5	5.30	13.6	1.75	9.96	1.46	450	121	571	
DS/LM5	60.7	165	21.7	94.5	25.9	7.25	34.1	4.97	22.8	4.11	10.7	1.36	7.53	1.05	368	94	462	
DS/LM6	62.0	172	22.1	95.9	26.6	7.08	32.2	4.67	21.9	4.07	10.1	1.27	7.03	1.03	379	89	468	
DS/LM7	9.64	14.6	1.34	4.68	0.758	0.171	1.09	0.122	0.475	0.09	0.203	0.022	0.072	0.008	31	2.3	33	
DS/LM8	90.4	550	26.0	109	25.8	7.03	37.2	5.34	26.3	4.70	11.6	1.44	7.37	1.14	801	102	903	
DS/CS1	0.026	0.066	0.009	0.036	0.003	0.007	0.006	—	0.004	—	—	0.003	—	0.140	0.020	0.160		
DS/CS2	0.034	0.074	0.013	0.077	—	0.010	0.013	0.003	0.006	0.002	0.002	—	—	0.200	0.040	0.230		
DS/CS3	0.723	1.30	0.142	0.582	0.090	0.031	0.160	0.019	0.069	0.014	0.039	0.003	0.023	0.003	2.8	0.4	3.2	
DS/CS4	0.263	0.422	0.041	0.182	0.018	0.012	0.049	0.006	0.021	0.006	0.012	0.002	0.011	—	0.9	0.1	1.1	
DS/AD1	37.0	126	15.3	70.0	23.7	6.13	27.0	3.74	15.9	2.77	7.09	0.858	4.52	0.768	272	69	341	

WS wet season, DS dry season, *LT1* Seepage Collection Tank, *LM2–8* acidic ponds, *LM4–8* Wetlands from the passive treatment system, *CS1–4* Corona Stream, *AD1* acidic seepage
 Σ LREE = sum of concentration of light REE (LREE: La to Sm); Σ HREE = sum of concentration of heavy REE (HREE: Eu to Lu); Σ REE = sum of total concentration of REE

Total and Dissolved REE Concentrations

The total concentrations of REE in the acidic ponds and throughout the PTS, ranged from $116 \mu\text{g L}^{-1}$ to $577 \mu\text{g L}^{-1}$ between the two seasons. The concentrations of REE in the first aeration pond (LM4) is attributed to the input of acidic water between the seepage collection tank (LT1) and the acidic lagoons (LM2, LM3) that takes place in this pond. As expected, the concentrations of REE, both total and dissolved, increased during the dry season due to evaporation.

Overall, the samples from the Corona Stream had low concentrations of total and dissolved REE, as expected for non-polluted rivers (e.g. Sholkovitz 1995; Zdzisław and Agnieszka 2015). During the wet season, the sum of dissolved REE increased from $0.08 \mu\text{g L}^{-1}$ (WS/CS2) to $15.1 \mu\text{g L}^{-1}$ (WS/CS3), most probably after the input of acidic seepage in the mine area, and to $46.9 \mu\text{g L}^{-1}$ (WS/CS4) after the confluence with the PTS effluent. A different behaviour was observed during the dry season, when there was no inflow of water from the PTS, so the total and dissolved concentrations of REE were lower than in the wet season. Nonetheless, there was an increase after the discharge of the acidic seepage (DS/AD1), leading to higher REE concentrations in the Corona River than before the PTS confluence (DS/CS3); since there was no outflow from the PTS, the lower contents in sample DS/CS4 may be due to attenuation.

The behaviour of La, Gd, and Yb throughout the AMD, PTS, and after the confluence with the Corona Stream (CS4) for both seasons is shown in Fig. 3. The three REE are broadly representative of the LREE, MREE, and HREE behaviour, respectively. In the acidic ponds and among the PTS, the ΣREE transport was carried out by the dissolved phase during the wet season (Fig. 3a), as previously reported (e.g. Cánovas et al. 2018; Olías et al. 2018). The dissolved

REE concentrations remained similar throughout the passive treatment system with a mean of $221 \mu\text{g L}^{-1}$ (samples WS/LM2 to WS/LM8) (Fig. 3a). The highest concentration was associated with the seepage collection tank (sample WS/LT1).

The highest REE concentrations in the AMD and PTS followed the pattern of $\text{Ce} > \text{Nd} > \text{La}$, both in the wet and dry seasons. However, sample DS/LM7 showed a different tendency, decreasing from $212 \mu\text{g L}^{-1}$ ΣREE dissolved concentration in the wet season to a ΣREE dissolved concentration of $33.3 \mu\text{g L}^{-1}$. When compared with the total concentration, most was transported as particulate matter (Fig. 3b). The behaviour of REE in the remaining samples was conservative due to the low pH conditions ($\text{pH} < 3$) and thus being transported in the dissolved phase. In the last wetland (DS/LM8), there was an increase in the concentration of dissolved REE, from $243 \mu\text{g L}^{-1}$ (wet season) to $903 \mu\text{g L}^{-1}$ (dry season), the highest concentration found in the area for both seasons (Fig. 3b). There was no water flowing from DS/LM7 to the remaining wetlands, so the increase was due to evaporation.

When comparing the ratio between the dissolved and total concentrations, the transport of REE mainly took place in the dissolved aliquot in acidic water and in the total aliquot in circumneutral water in both seasons (Fig. 4). During the wet season, two patterns were displayed in the samples collected from the Corona Stream. The LREE were predominant in the total fraction in the samples catalogued as background (WS/CS1, WS/CS2), but after the mixing with acidic waters from the acidic seepage and PTS, there was an enrichment of HREE in the total fraction (WS/CS3, WS/CS4) (Fig. 4a). In the dry season, even though the patterns were not as clear as in the first campaign, the REE behaviour of the last two sampling points was similar, with an enrichment of HREE

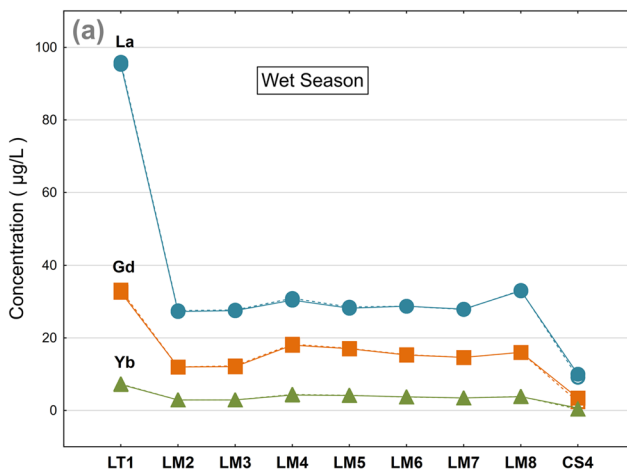
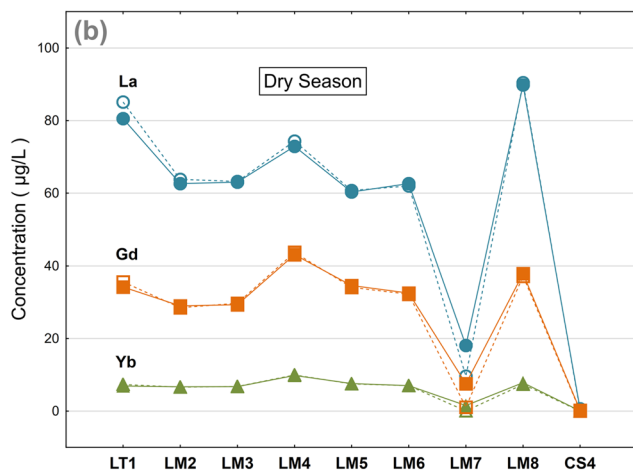


Fig. 3 Total (solid line and filled marker) and dissolved (dash line and open marker) concentration of La, Gd, and Yb throughout the passive treatment system up to the confluence with the Corona Stream for



both wet (a) and dry (b) season. LT1 Seepage Collection Tank, LM2–3 Acidic Ponds, LM4–8 Wetlands from the passive treatment system, CS4 Corona Stream after the confluence of the PTS

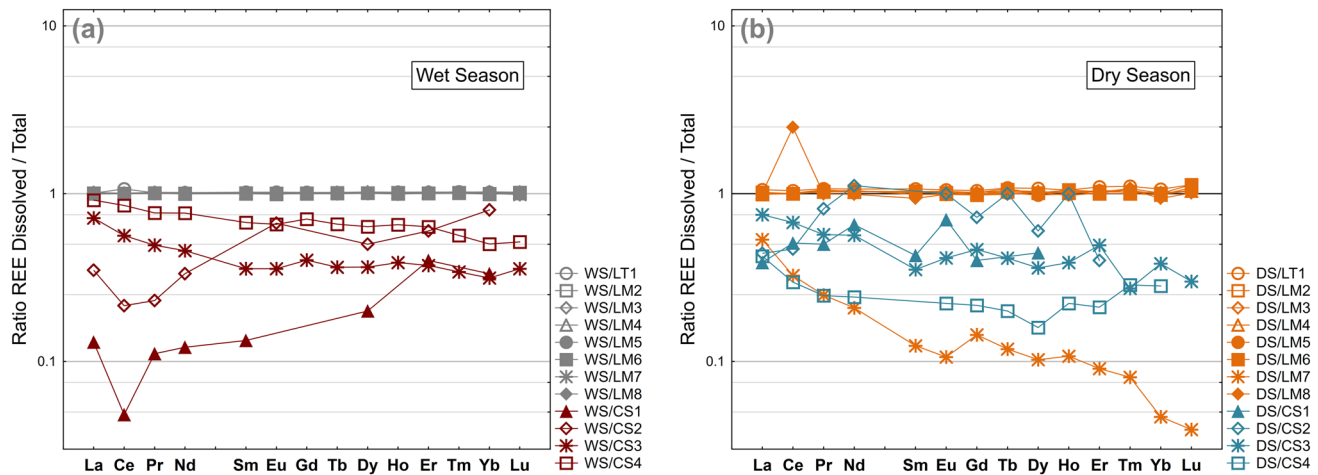


Fig. 4 Ratio between the dissolved and total concentration of REE in water samples collected during the wet (a) and dry (b) season in Lousal mine area, Portugal. WS wet season, DS dry season, LT1

Seepage Collection Tank, LM2-3 acidic ponds, LM4-8 Wetlands from the passive treatment system, CS1-4 Corona Stream, AD1 Acidic Seepage

in the total fraction (DS/CS3, DS/CS4). Most of the REE were present in the total fraction in the samples collected as background (DS/CS1, DS/CS2), especially the LREE. However, sample DS/CS2 had higher concentrations of Nd, Eu, Tb, and Er in the dissolved fraction (Fig. 4b).

Sample DS/LM7 had a different pattern from those observed in the PTS, which could be due to its higher pH (5.2), and a lower calculated Eh (311 mV), compared to the remaining PTS basins (average pH = 2.5 and calculated Eh = 736 mV). Besides, the design of this basin is different from the other aerobic wetlands, having only calcareous rocks beneath the topsoil. The topsoil reduces the oxygen in the water and the precipitation of iron oxides. While the water percolates and contacts the limestone, the pH increases, and the anoxic conditions favour the precipitation of other metals, such as Al (Hedin et al. 1994; Skousen et al. 2017). All of the REE were found in the total fraction of the water sample and the concentration increased with increasing atomic number across the REE, similar to the behaviour reported by Verplanck et al. (2004) in samples collected downstream from acid water input with circumneutral pH.

REE Partitioning Between Dissolved and Particulate Matter

Comparing samples collected from the wet season in the Lousal mine area, two distinct patterns can be observed in the samples collected from the AMD and PTS, and the samples from the Corona Stream. In the samples collected from the AMD and PTS, all the REE were in the dissolved fraction, while in the Corona Stream samples, the REE were

in the particulate matter. When the acidic waters from the AMD and PTS mixed with the circumneutral water from the Corona Stream (WS/CS4), the total concentrations of REE diminished and up to 20% of the transport of the REE took place as particulate matter. However, the partitioning and percentage of particulate matter of REE vary between the background samples (WS/CS1 and WS/CS2) and the samples affected by the acidic seepage and PTS outflow (WS/CS3 and WS/CS4).

As aforementioned, samples WS/CS1 and WS/CS2 had the lowest concentrations of REE but a high percentage of REE in the particulate matter, from 20 to 100%, with the lowest concentrations for Er and Yb. After the input of the acidic seepage (WS/CS3), the pH decreased to 5.5 and the concentrations of REE increased, although the percentage of the REE in the particulate matter decreased, from 28% (La) to 69% (Yb). Thus, there was a change in the partitioning pattern, the lowest percentages were associated with the LREE whilst the MREE and HREE had consistently higher percentages, with an average of 64%. After the outflow of the PTS (WS/CS4), the trend continued with a pH decrease to 5.2, and increased concentration of ΣREE, with a lower percentage as particulate matter. The percentage of particulate matter was higher for the HREE (39%, on average) than for LREE (21%). The lowest was 9% (La) and the highest was 50% (Yb).

Significant differences were observed in the samples collected during the dry season. The percentage of REE in the particulate matter increased at specific points in the AMD and throughout the PTS (e.g. DS/LM5 and DS/

LM8), and without a PTS outflow, the behaviour of the REE changed in the last point measured in the Corona Stream (DS/CS4). The samples from the AMD and PTS exhibited low percentages of REE associated with particulate matter (< 6%), except in sample DS/LM7, which ranged between 47% (La) and 96% (Lu). As seen in the acidic seepage and PTS outflow in the previous season (WS/CS3 and WS/CS4), there was a partitioning of the REE, with a strong preference of HREE over LREE.

For samples collected in the Corona Stream, sample DS/CS3 maintained the same fractionation pattern observed in the previous campaign due to the constant input of the acidic seepage. The sample had a higher percentage of particulate matter for the HREE (an average of 61%), and the lowest percentage attributed to La (25%). As previously mentioned, the lack of outflow from the PTS changed the amount of particulate matter, which increased, suggesting that the REE was mostly being transported as suspended matter. The overall concentration of REE decreased at this point and the percentage of particulate matter ranged from 58% (La) up to 100% (Lu).

Both white and reddish precipitates were observed during the sampling campaigns, in samples WS/CS3 and WS/CS4 in the wet season, and in sample DS/LM7 in the dry season. These samples had high concentrations of Fe and Al (supplemental Table S-1), mostly in the particulate matter (> 95%), and high sulphate concentrations (from 560 mg L⁻¹ in sample WS/CS3 up to 2200 mg L⁻¹ in sample DS/LM7), suggesting the presence of Al and Fe hydroxysulphates in the particulate suspended matter. Semiquantitative analysis performed in the filters from these samples corroborate the presence of basaluminite, gypsum, and Al hydroxysulphates

in sample DS/LM7, and basaluminite and Fe and Al hydroxysulphates in samples WS/CS3 and WS/CS4.

When plotting the partition coefficient, obtained by normalizing the concentration of REE in the particulate matter to the concentration of REE in the dissolved fraction, the fractionation pattern shows the M-type tetrad effect described by Matsuda et al. (1987) and Bau (1999) (Fig. 5). As reported by Lozano et al. (2019), in areas where there is mixing of water, such as sample WS/CS4, these Fe and Al phases are responsible for the removal of REE from solution, though it is affected by the pH. At circumneutral pH, basaluminite can retain REE (Lozano et al. 2019). From the distribution pattern, there appears to be a preferential fixation of HREE and MREE onto the Al and Fe precipitates (Fig. 5). This behaviour, reported by several authors (e.g. Ayora et al. 2016; Ferreira da Silva et al. 2009; Gammons et al. 2005; Lozano et al. 2019; Olías et al. 2018; Prudêncio et al. 2015; Verplanck et al. 2004), can also be applied to a certain extent to sample WS/CS3. Even though no sample was collected from the acidic seepage in Autumn in the first sampling campaign, the input is assumed, and the higher flux seen in the Spring could explain the higher concentration and the distribution pattern observed at this point.

REE PAAS-Normalized Distribution Pattern

The dissolved REE concentrations were normalized by the estimated average composition of the PAAS values (Nance and Taylor 1976). The normalized patterns of the AMD, PTS, and Corona Stream for Autumn and Spring are presented in Fig. 6. The normalized concentration ratios of $(La/Yb)_N < 1$ and similar $(La/Gd)_N < 1$ in the AMD and PTS samples denote an enrichment of HREE relative to LREE, and MREE enriched waters in both seasons (Table 3). The REE exhibit the characteristic convex-up concentration patterns (Fig. 6a,b) reported by several authors in acidic waters (e.g. Ferreira da Silva et al. 2009; Olías et al. 2018; Verplanck et al. 1999, 2004). The distribution patterns are similar in both campaigns despite the concentration differences, which suggests that the patterns are independent of the REE concentration, as previously observed by Ferreira da Silva et al. (2009) in the Lousal area.

Sample DS/LM7 exhibited a different behaviour from the aforementioned for AMD and PTS water, with an enrichment of LREE relative to MREE and HREE with $(La/Yb)_N > 1$ and $(La/Gd)_N > 1$ in the dissolved fraction (Table 3). Comparing the distributional patterns of the dissolved fraction and the total and particulate matter, a different behaviour is displayed (Fig. 7). As mentioned before, most of the REE are found in the particulate matter in the Corona Stream downstream of the mixing zone, and as the atomic number increases across the REE, the difference in concentrations increased as well. The total and particulate fraction were

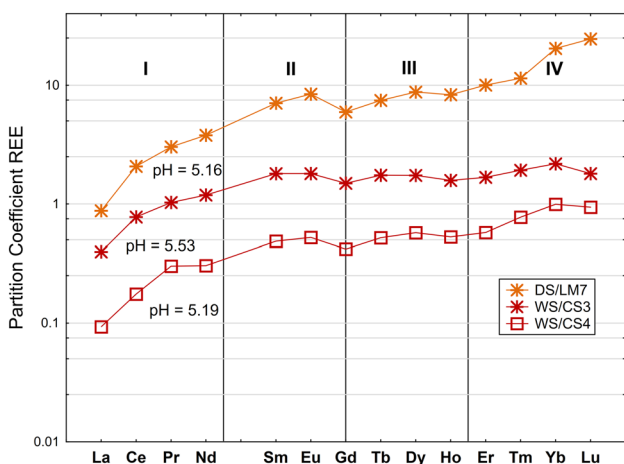


Fig. 5 Partition coefficient in the particulate matter showing the lanthanide M-type tetrad effect in samples DS/LM7, WS/CS3, and WS/CS4 from Lousal mine, Portugal. Partition coefficient calculated by normalizing the concentration of REE in the particulate matter to the dissolved concentration

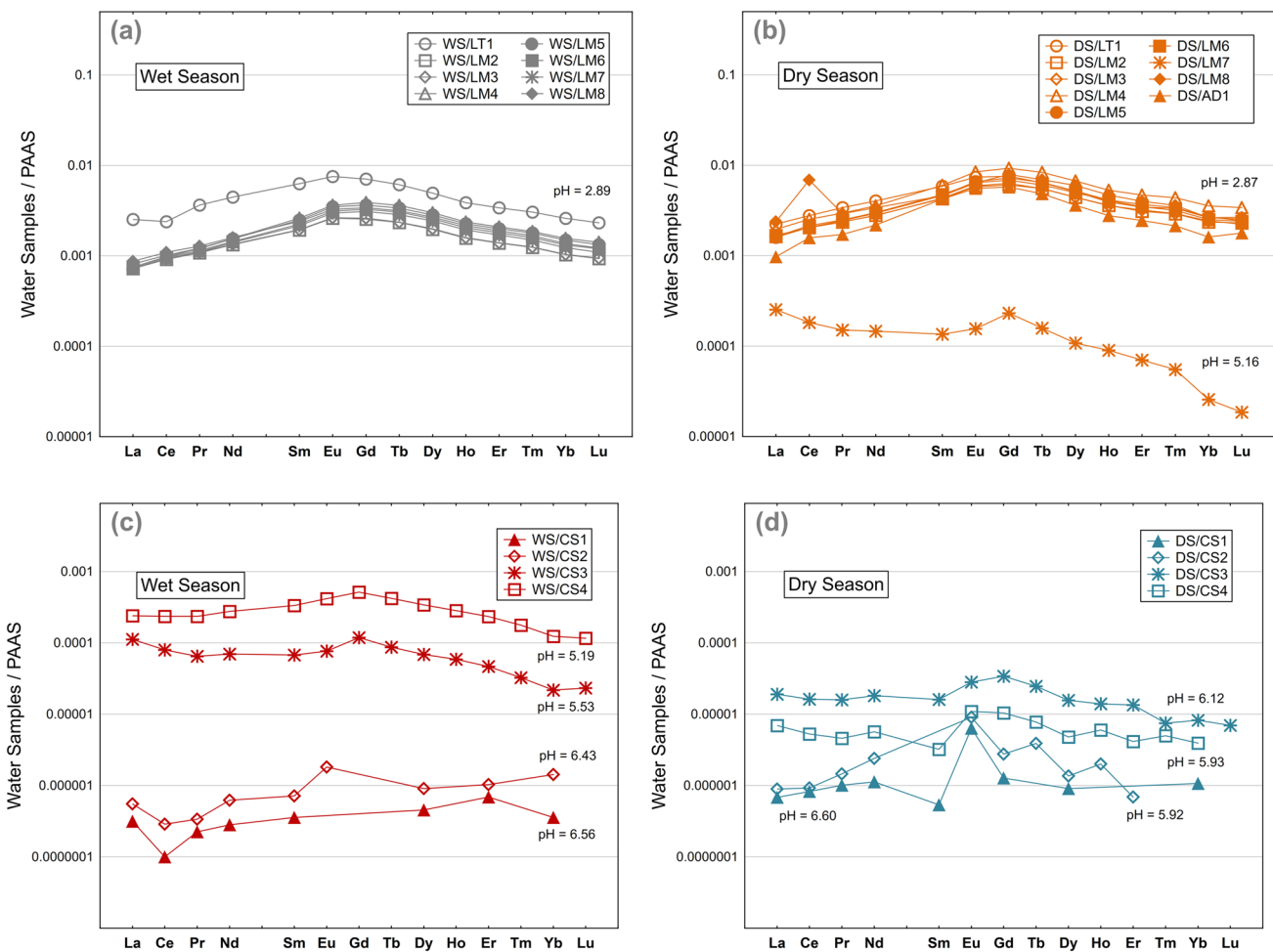


Fig. 6 PAAS-normalized REE distribution patterns of dissolved fraction of water samples from Lousal mine area, Portugal: AMD and PTS samples collected in autumn (a) and spring (b); Corona Stream samples collected in autumn (c) and spring (d)

enriched in MREE relative to LREE and HREE. This scavenging of REE from the total concentration is attributed to adsorption or co-precipitation onto the Al and Fe precipitates, yielding HREE enrichment in the particulate matter (Fig. 7).

The Corona Stream is slightly enriched in MREE in comparison to the LREE with $(La/Gd)_N < 1$ (Table 3). Before the confluence, the water is enriched in HREE relative to LREE with $(La/Yb)_N < 1$ (samples WS/CS1, WS/CS2, and DS/CS1). After the seepage of the acidic stream (WS/CS3, DS/CS3) and the PTS (WS/CS4, DS/CS4) the LREE were enriched relative to the HREE in both seasons with $(La/Yb)_N > 1$ (Table 3). These two distinctive patterns are well observed in the wet season (Fig. 6c).

The PAAS normalized patterns of the total, dissolved, and particulate fraction of samples CS3 and CS4 in both seasons

are shown in Fig. 8. Sample CS3 had a similar enrichment of LREE and MREE relative to HREE in both seasons in the total and dissolved fraction (Fig. 8a). However, the particulate was enriched in MREE relative to LREE and HREE, displaying a convex-up pattern in the wet season, and enriched in MREE and HREE relative to LREE in the dry season.

The distribution patterns of the total and dissolved fractions of sample CS4 in the wet season were enriched in MREE; meanwhile, the particulate matter was enriched in MREE and HREE compared to LREE (Fig. 8b). Considering that most of the REE is found in the particulate matter during the dry season, there is a similarity between the total and particulate fraction distribution pattern. Both are enriched in MREE relative to LREE and HREE, and the dissolved fraction is enriched in MREE.

Table 3 Seasonal distribution of Ce/Ce*, and Eu/Eu* anomalies, and normalized concentration ratios of $(La/Yb)_N$ and $(La/Gd)_N$ in the dissolved fraction of water samples from the acidic ponds, passive treatment system, acidic seepage, and Corona Stream of Lousal mine area, Portugal

Sample	Ce/Ce*	Eu/Eu*	$(La/Yb)_N$	$(La/Gd)_N$	Sample	Ce/Ce*	Eu/Eu*	$(La/Yb)_N$	$(La/Gd)_N$
WS/LT1	0.8	1.1	1.0	0.4	DS/LT1	1.0	1.1	0.9	0.3
WS/LM2	1.0	1.2	0.7	0.3	DS/LM2	1.0	1.1	0.7	0.3
WS/LM3	1.0	1.2	0.7	0.3	DS/LM3	1.0	1.1	0.7	0.3
WS/LM4	1.0	1.1	0.5	0.2	DS/LM4	1.1	1.1	0.6	0.2
WS/LM5	1.0	1.2	0.5	0.2	DS/LM5	1.1	1.1	0.6	0.2
WS/LM6	1.0	1.2	0.6	0.2	DS/LM6	1.1	1.1	0.7	0.2
WS/LM7	1.0	1.2	0.6	0.2	DS/LM7	0.9	0.9	9.9	1.1
WS/LM8	1.0	1.1	0.6	0.3	DS/LM8	2.6	1.1	0.9	0.3
WS/CS1	0.4	–	0.9	–	DS/CS1	1.0	7.7	0.6	0.5
WS/CS2	0.7	–	0.4	–	DS/CS2	0.8	–	–	0.3
WS/CS3	0.9	0.9	5.2	0.9	DS/CS3	0.9	1.2	2.3	0.6
WS/CS4	1.0	1.0	2.0	0.5	DS/CS4	0.9	1.9	1.8	0.7
					DS/AD1	1.2	1.1	0.6	0.2

WS wet season, DS dry season, LT1 Seepage Collection Tank, LM2-3 acidic ponds, LM4-8 Wetlands from the passive treatment system, CS1-4 Corona Stream, AD1 acidic seepage

Ce/Ce* = Ce anomaly calculated by the formula $Ce/Ce* = [(Ce_N)/(\sqrt{(La_N*Pr_N)})]$ (Worral and Pearson (2001)); Eu/Eu* = Eu anomaly calculated by the formula $Eu/Eu* = [(Eu_N)/(\sqrt{(Sm_N*Gd_N)})]$ (Worral and Pearson (2001)); $(La/Yb)_N$ and $(La/Gd)_N$ are normalized concentration ratios. La_N , Ce_N , Pr_N , Sm_N , Eu_N , Gd_N , and Yb_N are normalized values to PAAS (Nance and Taylor 1976)

Conclusions

The concentrations of total and dissolved REE in the water samples collected throughout the PTS and acidic ponds were similar in both seasons. Higher concentrations of REE occurred during the dry season and were associated with less precipitation and run-off, and evaporation throughout the PTS. During the wet season, there was a reduction in the REE concentrations, especially in the dissolved fraction, after the confluence with the Corona Stream, which might

be due to dilution. The total and dissolved concentrations of REE in the Corona Stream was lower during the dry season due to a lack of outflow from the PTS.

In the AMD and throughout the PTS, the REE behave conservatively because of the acidic pH ($pH < 3$), with all of the REE being dissolved. In contrast, where mixing of acidic and circumneutral waters occurs (CS3, CS4), the pH increased ($pH > 5$) and the REE were partially removed from solution. The scavenging and partitioning of REE can be attributed to the formation of Al and Fe precipitates due to the increased pH. Sorption onto these precipitates is not uniform across the REE, with a depletion of LREE and a preferential fixation of HREE.

The REE PAAS-normalized distribution patterns from the AMD and PTS dissolved water samples show the characteristic convex-up enrichment in MREE relative to LREE and HREE reported by several authors in acidic waters. The distribution pattern is different in the two seasons, even though the concentration is higher in the dry season, corroborating that the patterns are independent of the concentration. Background REE distribution patterns in the Corona Stream exhibit an enrichment of HREE relative to LREE; after the acidic seepage and PTS effluent enters the stream, an enrichment of LREE relative to HREE occurs in both the wet and dry seasons.

The results obtained in this first work focused on REE distribution and behaviour in water in the Lousal mine area and throughout the PTS are an important benchmark for further studies. In fact, REE can play a significant role as tracers of the remediation processes, yielding a better understanding

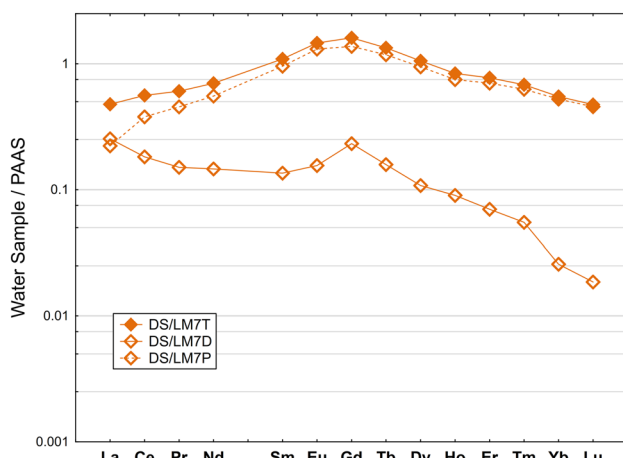


Fig. 7 PAAS-normalized REE distribution patterns of the total, dissolved and particulate fraction of sample DS/LM7. T total represented with a solid line and full marker; D dissolved represented with a solid line and open marker; P particulate matter represented with dashed line and open marker

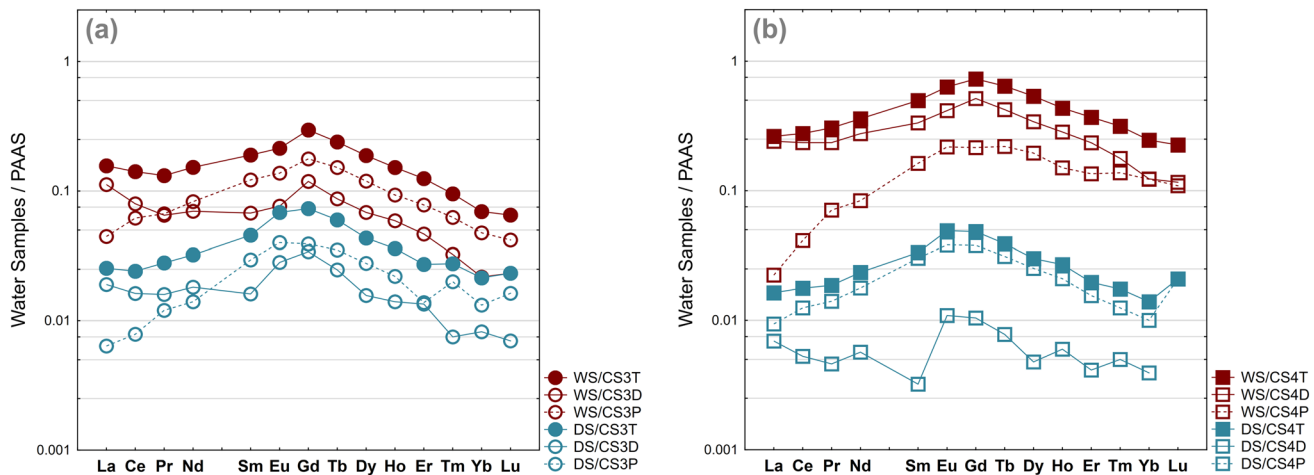


Fig. 8 PAAS-normalized REE distribution patterns of the total, dissolved and particulate fraction of samples CS3 (a) and CS4 (b) in autumn and spring. *T* total represented with a solid line a full marker, *D* dissolved represented with a solid line and open marker, *P* particulate matter represented with dashed line and open marker

of the complexity of hydrogeochemical processes that can occur in a PTS.

Supplementary Information The online version contains supplementary material available at <https://doi.org/10.1007/s10230-023-00954-2>.

Acknowledgements ITN PANORAMA – This project has received funding from European Union's Horizon 2020 research and innovation program under the Marie Skłodowska-Curie Grant 857989. The authors also thank the reviewers for all of their suggestions.

Funding Open access funding provided by FCT|FCCN (b-on).

Data availability Study data is available in the tables within the paper and in the Supplemental Information accompanying the on-line version of this paper.

Open Access This article is licensed under a Creative Commons Attribution 4.0 International License, which permits use, sharing, adaptation, distribution and reproduction in any medium or format, as long as you give appropriate credit to the original author(s) and the source, provide a link to the Creative Commons licence, and indicate if changes were made. The images or other third party material in this article are included in the article's Creative Commons licence, unless indicated otherwise in a credit line to the material. If material is not included in the article's Creative Commons licence and your intended use is not permitted by statutory regulation or exceeds the permitted use, you will need to obtain permission directly from the copyright holder. To view a copy of this licence, visit <http://creativecommons.org/licenses/by/4.0/>.

References

Alpers C, Blowes DW, Nordstrom DK, Jambor JL (1994) Secondary minerals and acid mine-water chemistry. In: Blowes JL, Jambor DW (eds), Short Course Handbook on Environmental Geochemistry of Sulfide Mine Wastes, Mineralogical Assoc of Canada, Waterloo, pp 247–270

Åström ME, Nystrand M, Gustafsson JP, Österholm P, Nordmyr L, Reynolds JK, Peltola P (2009) Lanthanoid behaviour in an acidic landscape. *Geochim Cosmochim Acta* 74:829–845. <https://doi.org/10.1016/j.gca.2009.10.041>

Ayora C, Macías F, Torres E, Lozano A, Carrero S, Nieto JM, Pérez-López R, Fernández-Martínez A, Castillo-Michel H (2016) Recovery of rare earth elements and yttrium from passive remediation systems of acid mine drainage. *Environ Sci Technol* 50:8255–8262. <https://doi.org/10.1021/acs.est.6b02084>

Bau M (1999) Scavenging of dissolved yttrium and rare earths by precipitating iron oxyhydroxide: experimental evidence for Ce oxidation, Y-Ho fractionation, and lanthanide tetrad effect. *Geochim Cosmochim Acta* 63(1):67–77. [https://doi.org/10.1016/S0016-7037\(99\)00014-9](https://doi.org/10.1016/S0016-7037(99)00014-9)

Câmara Municipal de Grândola (2012) Plano municipal de emergência de protecção civil de Grândola. Parte IV-Informação complementar. Secção II Análise de riscos

Cánovas C, Olías M, Nieto J, Sarmiento A, Cerón J (2006) Hydrogeochemical characteristics of the Tinto and Odiel Rivers (SW Spain). Factors controlling metal contents. *Sci Total Environ* 373:363–382. <https://doi.org/10.1016/j.scitotenv.2006.11.022>

Cánovas C, Riera J, Carrero S, Olías M (2018) Dissolved and particulate metal fluxes in an AMD-affected stream under different hydrological conditions: The Odiel River (SW Spain). *CATENA* 165:414–424. <https://doi.org/10.1016/j.catena.2018.02.020>

Fernandez-Caliani JC, Barba-Brioso C, De la Rosa JD (2009) Mobility and speciation of rare earth elements in acidic minesoils and geochemical implications for river waters in the southwestern Iberian margin. *Geoderma* 149:393–401. <https://doi.org/10.1016/j.geodrma.2009.01.004>

Ferreira da Silva E, Fonseca EC, Matos JX, Patinha C, Reis P, Santos Oliveira JM (2005) The effect of unconfined mine tailings on the geochemistry of soils, sediments and surface waters of the Lousal area (Iberian Pyrite Belt, southern Portugal). *Land Degrad Dev* 16(2):213–228. <https://doi.org/10.1002/ldr.659>

Ferreira da Silva E, Patinha C, Reis P, Fonseca EC, Matos JX, Barrosinho J, Oliveira JM (2006) Interaction of acid mine drainage with waters and sediments at the Corona stream, Lousal mine (Iberian Pyrite Belt, southern Portugal). *Environ Geol* 50(7):1001–1013. <https://doi.org/10.1007/s00254-006-0273-6>

Ferreira da Silva E, Bobos I, Matos JX, Patinha C, Reis AP, Fonseca EC (2009) Mineralogy and geochemistry of trace metals and REE in volcanic massive sulfide host rocks, stream sediments, stream waters and acid mine drainage from the Lousal mine area (Iberian Pyrite Belt, Portugal). *Appl Geochem* 24:383–401. <https://doi.org/10.1016/j.apgeochem.2008.12.001>

Gammons CH, Wood SA, Pedrozo F, Varekamp JC, Nelson BJ, Shope CL, Baffico G (2005) Hydrogeochemistry and rare earth element behavior in a volcanically acidified watershed in Patagonia, Argentina. *Chem Geol* 222:249–267. <https://doi.org/10.1016/j.chemgeo.2005.06.002>

Gromet LP, Haskin LA, Korotev RL, Dymek RF (1984) The “North American shale composite”: its compilation, major and trace element characteristics. *Geochim Cosmochim Acta* 48(12):2469–2482. [https://doi.org/10.1016/0016-7037\(84\)90298-9](https://doi.org/10.1016/0016-7037(84)90298-9)

Hedin RS, Nairn RW, Kleinmann RLP (1994) Passive treatment of coal mine drainage. IC 9389, U.S. Bureau of Mines, Washington, DC

Henderson P (1984) General geochemical properties and abundances of the rare earth elements. In: Henderson P (ed) *Developments in geochemistry*, vol 2, Elsevier, Amsterdam

International Union of Pure and Applied Chemistry (IUPAC) (2005) Nomenclature of Inorganic Chemistry, IUPAC Recommendations. In: Connelly NG, Damhus T, Hartshorn RM, Hutton AT (eds) *IUPAC Red Book*, prepared for publication. RSC Publishing (ISBN 0 85404 438 8)

Johannesson KH, Lyons WB (1995) Rare-earth element geochemistry of Colour Lake, an acidic freshwater lake on Axel Heiberg Island, Northwest Territories, Canada. *Chem Geol* 119:209–223. [https://doi.org/10.1016/0009-2541\(94\)00099-T](https://doi.org/10.1016/0009-2541(94)00099-T)

Johannesson KH, Zhou X (1999) Origin of middle rare earth element enrichments in acid waters of a Canadian High Arctic lake. *Geochim Cosmochim Acta* 63:153–165. [https://doi.org/10.1016/S0016-7037\(98\)00291-9](https://doi.org/10.1016/S0016-7037(98)00291-9)

Leybourne MI, Johannesson KH (2008) Rare earth elements (REE) and yttrium in stream waters, stream sediments, and Fe-Mn oxyhydroxides: fractionation, speciation, and controls over REE+Y patterns in the surface environment. *Geochim Cosmochim Acta* 72:5962–5983. <https://doi.org/10.1016/j.gca.2008.09.022>

Li X, Wu P (2017) Geochemical characteristics of dissolved rare earth elements in acid mine drainage from abandoned high-As coal mining area, southwestern China. *Environ Sci Pollut R* 24(25):20540–20555. <https://doi.org/10.1007/s11356-017-9670-5>

Life Ribermine (2021) New weather station in Lousal contributes to the local and regional climate knowledge. IOP Publishing Life Ribermine. <https://liferibermine.com/en/2021/12/22/new-weather-station-in-Lousal-contributes-to-the-local-and-regional-climate-knowledge/> Accessed 23 Jan 2023

Lozano A, Ayora C, Fernández-Martínez A (2019) Sorption of rare earth elements onto basaluminite: the role of sulfate and pH. *Geochim Cosmochim Acta* 258:50–62. <https://doi.org/10.1016/j.gca.2019.05.016>

Luís AT, Teixeira P, Pinheiro Almeida SF, Matos JX, Ferreira da Silva E (2011) Environmental impact of mining activities in the Lousal area (Portugal): chemical and diatom characterization of metal-contaminated stream sediments and surface water of Corona Stream. *Sci Total Environ* 409:4312–4325. <https://doi.org/10.1016/j.scitotenv.2011.06.052>

Matos JX, Oliveira V (2003) Mina do Lousal (Faixa Piritosa Ibérica) – Percurso geológico e mineiro pelas cortas e galerias da antiga mina. IGME, Pub. Museo Geominero nº2, Espanha, pp 117–128

Matsuda A, Kawakami O, Dohmoto Y, Takenaka T (1987) Lanthanide tetrad effects in nature: two mutually opposite types, W and M. *Geochem J* 21:119–124. <https://doi.org/10.2343/geochemj.21.119>

Nance WB, Taylor SR (1976) Rare earth element patterns and crustal evolution—I. Australian post-Archean sedimentary rocks. *Geochim Cosmochim Acta* 40(12):1539–1551. [https://doi.org/10.1016/0016-7037\(76\)90093-4](https://doi.org/10.1016/0016-7037(76)90093-4)

Noack CW, Dzombak DA, Karamalidis AK (2014) Rare earth element distributions and trends in natural waters with a focus on groundwater. *Environ Sci Technol* 48:4317–4326. <https://doi.org/10.1021/es4053895>

Olías M, Cánovas CR, Basallote MD, Lozano A (2018) Geochemical behaviour of rare earth elements (REE) along a river reach receiving inputs of acid mine drainage. *Chem Geol* 493:468–477. <https://doi.org/10.1016/j.chemgeo.2018.06.029>

Oliveira JS, Farinha J, Matos JX, Ávila P, Rosa C, Machado MC, Daniel FS, Martins L, Leite MM (2002) Diagnóstico ambiental das principais áreas mineiras degradadas do país. Boletim de Minas 39, Lisboa, pp 67–85

Plumlee GS, Smith KS, Montour MR, Ficklin WH, Mosier EL (1999) Geologic controls on the composition of natural waters and mine waters draining diverse mineral-deposit types. *The Environmental Geochemistry of Mineral Deposits, Part B. Case Studies and Research Topics*. Rev Econ Geol 6B, Society of Economic Geologists, Littleton, pp 373–432.

Prudêncio MI, Valente T, Marques R, Braga MA, Pamplona J (2015) Geochemistry of rare earth elements in a passive treatment system built for acid mine drainage remediation. *Chemosphere* 138:691–700. <https://doi.org/10.1016/j.chemosphere.2015.07.064>

Sholkovitz ER (1995) The aquatic chemistry of rare earth elements in rivers and estuaries. *Aquat Geochem* 1(1):1–34. <https://doi.org/10.1007/BF01025229>

Skousen J, Zipper CE, Rose A, Ziemkiewicz PF, Nairn R, McDonald LM, Kleinmann RL (2017) Review of passive systems for acid mine drainage treatment. *Mine Water Environ* 36(1):133–153. <https://doi.org/10.1007/s10230-016-0417-1>

Strauss G (1970) Sobre la geología de la provincia piritífera del SW de la Península Ibérica y de sus yacimientos, en especial sobre la mina de pirita de Lousal (Portugal). Memórias Instituto Tecnológico GeoMinero España 77 (in Spanish)

Valente M, Antunes T, Sequeira Braga M, Prudêncio MI, Marques R, Pamplona J (2012) Mineralogical attenuation for metallic remediation in a passive system for mine water treatment. *Environ Earth Sci* 66:39–54. <https://doi.org/10.1007/s12665-011-1205-7>

Verplanck PL, Nordstrom DK, Taylor HE (1999) Overview of rare earth element investigations in acid waters of U.S. Geological Survey abandoned mine lands watersheds. U.S. Geological Survey Water-Resources Investigations Report 99-4018A, pp 83–92

Verplanck PL, Nordstrom DK, Taylor HE, Kimball BA (2004) Rare earth element partitioning between hydrous ferric oxides and acid mine water during iron oxidation. *Appl Geochem* 19:1339–1354. <https://doi.org/10.1016/j.apgeochem.2004.01.016>

Worrall F, Pearson D (2001) Water-rock interaction in an acidic mine discharge as indicated by rare earth element patterns. *Geochim Cosmochim Acta* 65:3027–3040. [https://doi.org/10.1016/S0016-7037\(01\)00662-7](https://doi.org/10.1016/S0016-7037(01)00662-7)

Zdziślaw MM, Agnieszka G (2015) The characteristics, occurrence, and geochemical behavior of rare earth elements in the environment: a review. *Crit Rev Environ Sci Technol* 45(5):429–471. <https://doi.org/10.1080/10643389.2013.866622>